Variable Exponent Lebesgue Space Inversion for Cross-Borehole Subsurface Imaging

Claudio Estatico, Alessandro Fedeli, Matteo Pastorino, and Andrea Randazzo

Abstract – A novel quantitative electromagnetic imaging method for subsurface prospecting is proposed in this article, exploiting the potentialities of the regularization theory in Lebesgue spaces with variable exponents. The described technique has been preliminarily validated by means of numerical simulations, where scattered field data are collected in a cross-borehole scenario.

1. Introduction

One of the most promising applications of electromagnetic imaging techniques is related to subsurface prospecting [1, 2]. At present, a significant number of methods have been developed and tested in various configurations. The majority of approaches rely on the qualitative processing of ground penetrating radar data acquired above the ground surface or in cross-borehole configurations [3–6]. Nevertheless, a correct interpretation of the data is usually a difficult task even for well-trained users, and it is not enough in several contexts, where a point-by-point determination of the dielectric properties of buried targets is required. However, the quantitative reconstruction of the underground structures is impaired by the presence of a stratified medium, which complicates the scattering phenomena significantly [7, 8]. In addition, the amount of data that can be collected in a traditional subsurface imaging configuration is usually less than its free-space counterpart, because of the difficulties in defining a set of measurement probes all around the region under test.

To address these challenging problems, the research community is continuously working toward the development of novel full-wave inversion strategies for buried object detection (e.g., the recently proposed virtual experiment framework [9, 10]), as well as for the improvement of existing ones in view of a practical application. In this context, nonlinear approaches exploiting Newton-type schemes seem to be promising. In particular, techniques exploiting the regularization theory in L^p Banach spaces have been found to be capable of substantially increasing the reconstruction accuracy in this applicative scenario [11, 12]. However, the selection of an adequate Lebesgue space exponent p remained a crucial issue until variable exponent microwave-imaging methods have been introduced [13]. In this article, the variable exponent approach is extended for the first time to deal with subsurface imaging configurations. Note that the main difference with respect to [13] is the use, inside the scattering model, of the proper two-dimensional (2D) Green's function for two-layer media. However, the presence of the ground–air interface makes the inverse problem significantly more difficult. Consequently, the present article is aimed at evaluating the regularization properties of the method in this more involved case. In particular, its capabilities have been assessed in an initial numerical framework, where a cross-borehole measurement technique has been taken into account.

Manuscript received 20 December 2019.

Claudio Estatico is with the Department of Mathematics, University of Genoa, via Dodecaneso 35, 16146 Genova, Italy; e-mail: estatico@dima.unige.it.

Alessandro Fedeli, Matteo Pastorino, and Andrea Randazzo are with the Department of Electrical, Electronic, Telecommunications Engineering and Naval Architecture, University of Genoa, via all'Opera Pia 11A, 16145 Genoa, Italy; e-mail: alessandro.fedeli@unige.it, matteo.pastorino@unige.it, andrea.randazzo@unige.it.

2. Overview of the Mathematical Formulation

The electromagnetic problem is formulated in a 2D and scalar setting, whose geometry is exemplified in Figure 1. The method is developed in the frequency domain, with an $e^{j2\pi ft}$ time dependence (f denotes the considered frequency). The space is divided into two regions: the upper one is air (characterized by the dielectric permittivity of vacuum ϵ_0), whereas the lower half-space is a terrain whose complex permittivity is ϵ_1. A 2D underground domain in the xy plane constitutes the investigation region R_i, whose dielectric properties are assumed to be unknown and are retrieved by the inversion process. Two vertical boreholes, positioned at both sides of R_i, contain the antennas used to illuminate the scenario and to collect the scattered electric field. These boreholes constitute the measurement domain R_m. The z component of the scattered electric field E_{zs} in R_m is related to the dielectric properties of R_i by means of the nonlinear equation [14]

$$E_{zs}(\mathbf{r}) = \mathcal{L}_{R_m}\tau\left(I - \mathcal{L}_{R_i}\tau\right)^{-1}E_{zi}(\mathbf{r}), \quad \mathbf{r} \in R_m \tag{1}$$

where E_{zi} is the incident electric field and $\tau = (\epsilon - \epsilon_1)/\epsilon_1$ and $\mathcal{L}_R$ (with $R = \{R_i, R_m\}$) are linear integral operators whose definition is given by

$$\mathcal{L}_R a(\mathbf{r}) = -k_1^2 \iint_{R_i} a(\mathbf{r}')g_M(\mathbf{r}, \mathbf{r}')d\mathbf{r}', \ \mathbf{r} \in R. \tag{2}$$

In (2), k_1 is the wavenumber inside the lower half-space, and g_M is the 2D Green's function for a planar two-layer configuration [15]. (1) is written in a compact form as $E_{zs} = \mathcal{N}(\tau)$, where $\tau \in X$ is the unknown of the

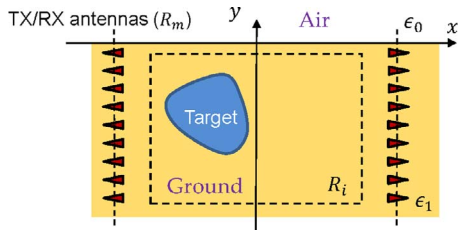

Figure 1. Configuration of the subsurface imaging problem.

problem and $E_{zs} \in Y$ represents the measured data, being X, Y, two Lebesgue functional spaces.

In our solving strategy, an iterative linearization of (1) around the current estimate of the solution τ is performed. At the kth iteration ($k = 1, \ldots, K$), the linear equation to be solved is $\mathcal{N}'_k h_k = E_{zs} - \mathcal{N}(\tau_k)$, where τ_k is the kth estimation of τ, $\mathcal{N}'_k$ is the Fréchet derivative of $\mathcal{N}$, and h_k is the unknown of the linearized problem. Once h_k is found, it is summed to τ_k to update the solution. The key point is represented by the regularizing approach adopted for the resolution of such a linear equation. In this article, we adopt a Landweber method formulated in Lebesgue spaces $L^{p(\cdot)}$ with variable exponents, whose ith iteration ($i = 1, \ldots, I$) is defined as

$$h_{k,i+1} = J_{X^*}\left[J_X\left(h_{k,i}\right) - \alpha \mathcal{N}'^*_k J_Y\left(\mathcal{N}'_k h_{k,i} - E_k\right)\right] \quad (3)$$

where $E_k = E_{zs} - \mathcal{N}(\tau_k)$ and $\mathcal{N}'^*_k$ is the adjoint of $\mathcal{N}'_k$ and $\alpha \in \mathbb{R}^+$. The functions J_X, J_{X^*}, and J_Y, called *duality maps*, are computed as in [13], by considering X as a variable exponent Lebesgue space and the space Y as a standard fixed exponent one. More precisely, X is an $L^{p(\mathbf{r})}$ space, with $\mathbf{r} \in R_i$, whereas Y is an L^{p_a} space, with p_a being the average value of $p(\mathbf{r})$ for $\mathbf{r} \in R_i$. In other words, the exponent $p(\mathbf{r})$ in the space of the unknown is a function of the position vector inside the investigation domain, and its value at the kth iteration ($p_k(\mathbf{r})$, $\mathbf{r} \in R_i$) depends on the magnitude of the reconstructed function at the previous linearization step τ_{k-1} as follows

$$p_k(\mathbf{r}) = p_m + \Delta p |\tau_{k-1}(\mathbf{r})| / \max_{\mathbf{r} \in R_i} |\tau_{k-1}(\mathbf{r})| \quad (4)$$

This means that for each point of R_i, the values of p_k lie in the interval $[p_m, p_m + \Delta p]$ and are linearly connected to the normalized magnitude of τ_{k-1}, which contains information about the locations of the buried targets. In the first linearization step, where τ_{k-1} is not available, p_1 is initialized to a constant value. Alternatively, it may be defined on the basis of a priori information.

3. Numerical Results

The developed inversion strategy has been initially tested in a numerically simulated scenario. In particular, a homogeneous dry ground has been assumed and modeled by a material with complex dielectric permittivity $\epsilon_1 = (4 - j0.6)\epsilon_0$. Two boreholes at $x_b = \pm 0.6\lambda_0$ have been considered, where λ_0 is the wavelength in vacuum. A total of $S = 22$ antennas (11 for each borehole) have been simulated in a multistatic–multiview arrangement. Each antenna acts, in turn, as a transmitter (a line source model is used), and the remaining ones (assumed as ideal field probes) collect the field. The investigation region R_i is a square domain with the side length $L_i = \lambda_0$ centered in $(0, -0.5\lambda_0)$. The working frequency has been set equal to $f = 300$ MHz.

The electromagnetic field is computed by using a custom forward solver on the basis of the method of moments (with pulse basis functions and Dirac delta weighting functions), in which the investigated scenario has been discretized into $N_{fw} = 40 \times 40$ square subdomains of side length $l = 2.5$ cm. Moreover, to obtain more realistic data, the computed values have been corrupted with a zero-mean Gaussian noise characterized by a signal-to-noise ratio of 30 dB.

In the inversion procedure, the investigation domain has been discretized into $N_{\mathrm{in}} = 30 \times 30$ square subdomains of side $l = 3.3$ cm to avoid inverse crimes. The parameters of the variable exponent inversion method are the following: $p_1 = 1.4$, $p_m = 1.2$, and $\Delta p = 0.8$. Moreover, both iterative loops are terminated when the relative variation of the data residual is less than a threshold $\Delta r_{\mathrm{th}} = 1\%$ or when the numbers of iterations exceed the predefined values of $K = 20$ (for the outer loop) and $I = 10$ (for the inner loop). Such values have been selected on the basis of the previous analyses performed in the free-space scenario. Indeed, it has been found that values of the norm exponent close to one produce better reconstructions of sparse regions (e.g., the background); thus, the lower bound of the exponent function $p(\cdot)$ has been set equal to $p_m = 1.2$. As a result, according to (4), low values of the exponent function are assigned to the background region. Conversely, values close to two allow a good reconstruction of smooth regions (e.g., the internal structure of the targets embedded in the subsoil). Therefore, the maximum value of $p(\cdot)$ has been set equal to $p_m + \Delta p = 2$. In the initial iteration, the exponent function has been empirically fixed to a constant value close to the lower bound (i.e., $p_1 = 1.4$).

In the first case, a single buried target is assumed, which is a void cylinder ($\epsilon = \epsilon_0$) with center $\mathbf{r}_c = (0.1, -0.6)\lambda_0$ and diameter $d_c = 0.3\lambda_0$. Figure 2 reports the resulting reconstructed distribution of the real and imaginary parts of the relative dielectric permittivity inside R_i obtained with the proposed approach. For comparison, the same scattered field data have been used to retrieve the permittivity distribution with an inexact Newton technique in L^p spaces with a fixed exponent [12], in which the predefined p parameter has been swept between 1.1 and 2 (the latter corresponding to a Hilbert space approach). The result of this analysis has been reported in Figure 3, where the average relative error on the reconstructed permittivity is shown for each fixed value of p versus the proposed methodology. According to this performance metric,

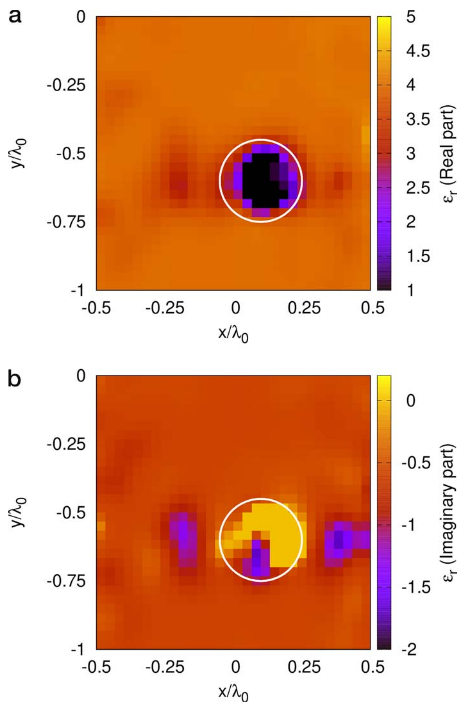

Figure 2. Reconstructed distribution of the (a) real and (b) imaginary parts of the relative dielectric permittivity in the first case (single void cylinder). Variable exponent approach.

the best fixed exponent results have been achieved for $p = 1.2$, where the error bottoms out at the value 0.145. The proposed approach produces a significant improvement in the reconstruction, with a relative error equal to 0.108. Incidentally, this is also a small value compared with the Hilbert space case ($p = 2$), where the error is 0.216. Figures 4 and 5 report the two dielectric reconstructions obtained for a fixed exponent space with $p = 1.2$ and in the Hilbert case, respectively.

The performance of the method has been also examined with respect to the size of the considered cylinder, for $d_c \in [0.1,\ 0.4]\lambda_0$. Table 1 shows that the reconstruction error grows together with an increase of d_c, which gives rise to more artifacts in the region R_i.

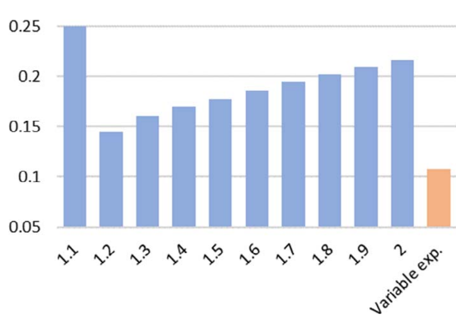

Figure 3. Relative reconstruction error obtained with the proposed variable exponent method versus the fixed exponent one with different values of p.

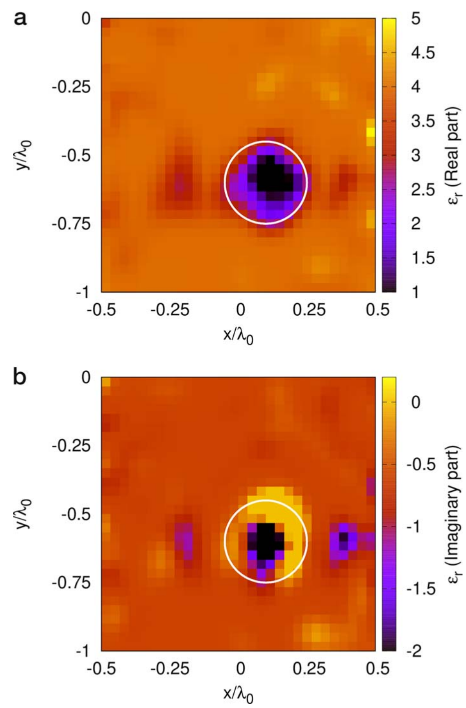

Figure 4. Reconstructed distribution of the (a) real and (b) imaginary parts of the relative dielectric permittivity in the first case (single void cylinder). Best result obtained with a fixed exponent method ($p = 1.2$).

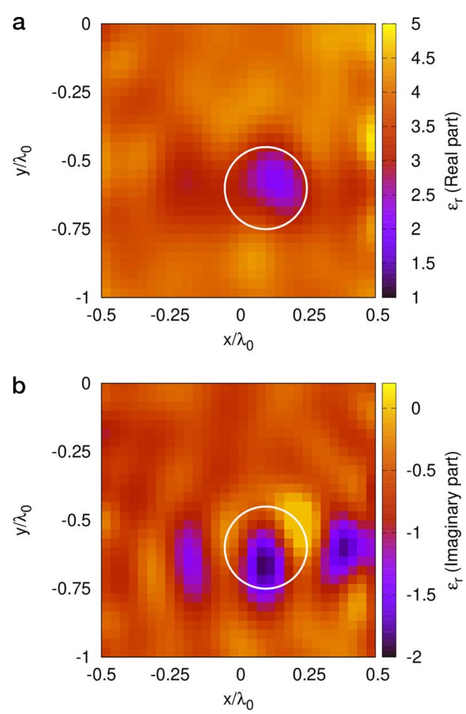

Figure 5. Reconstructed distribution of the (a) real and (b) imaginary parts of the relative dielectric permittivity in the first case (single void cylinder). Hilbert space result ($p = 2$).

Table 1. Relative reconstruction errors, number of performed outer iterations, and elapsed time for different diameters of the void cylinder

Cylinder diameter (m)	Reconstruction error	Iteration number	Time[a] (s)
0.1	0.022	2	49.73
0.2	0.079	3	59.73
0.3	0.108	4	70.73
0.4	0.181	13	176.18

[a] Elapsed time on a desktop PC equipped with a Quad-Core Intel i5-2310 CPU and 8 GB of RAM.

The number of performed outer iterations in each case, as well as the corresponding computational times are also reported in the table. An increase in both reconstruction time and the number of iterations is observed in the presence of larger buried objects.

As a further test scenario, a more complex configuration, including two different targets has been considered. The first target is a void circular cylinder ($\epsilon = \epsilon_0$) centered at $\mathbf{r}_c = (0.1, -0.6)\lambda_0$ and with diameter $d_c = 0.2\lambda_0$. The second object is a dielectric slab characterized by $\epsilon_r = 8$, centered at $\mathbf{r}_s = (-0.1, -0.25)\lambda_0$ and with sides $0.1\lambda_0$ and $0.4\lambda_0$. The real and imaginary parts of the relative dielectric permittivity reconstructed by means of the proposed strategy are shown in Figure 6. Figure 7 reports a comparison between the errors obtained with the variable exponent approach and the fixed exponent one, with $p \in [1.1, 2]$. As in the previous case, the

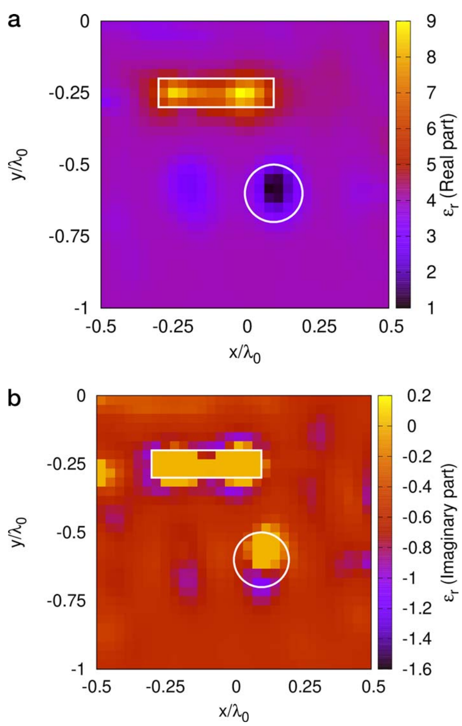

Figure 6. Reconstructed distribution of the (a) real and (b) imaginary parts of the relative dielectric permittivity in the second case (two buried targets). Variable exponent approach.

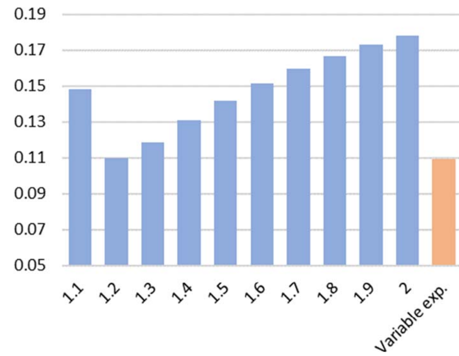

Figure 7. Relative reconstruction error obtained with the proposed variable exponent method versus the fixed exponent one with different values of p. Two buried targets.

results achieved by the novel method compare very well with the best ones given by the fixed exponent technique. However, note that the proposed approach avoids performing an external selection of the p parameter (for which the knowledge of the exact solution is necessary) because it is automatically defined inside the inversion process and adaptively updated iteration by iteration.

4. Conclusions

An inversion procedure developed in the framework of Lebesgue spaces with variable exponents has been considered in this article. For the first time, this kind of approach is applied to the quantitative dielectric reconstruction of buried structures, in which the problem is more challenging with respect to the free-space setting. The presented numerical results, obtained with a cross-borehole measurement configuration, demonstrate the potentialities of the proposed approach in the retrieval of the dielectric properties of the targets, also compared with the fixed exponent techniques.

5. References

1. D. J. Daniels, *Ground Penetrating Radar*. London, Institution of Electrical Engineers, 2004.
2. A. Benedetto and L. Pajewski, *Civil Engineering Applications of Ground Penetrating Radar*, Cham, Switzerland, Springer, 2015.
3. I. Catapano, A. Affinito, A. Del Moro, G. Alli, and F. Soldovieri, "Forward-Looking Ground-Penetrating Radar via a Linear Inverse Scattering Approach," *IEEE Transactions on Geoscience and Remote Sensing*, **53**, 10, October 2015, pp. 5624–5633.
4. R. Persico, *Introduction to Ground Penetrating Radar: Inverse Scattering and Data Processing*, Hoboken, NJ, Wiley, 2014.
5. F. Soldovieri, O. Lopera, and S. Lambot, "Combination of Advanced Inversion Techniques for an Accurate Target Localization via GPR for Demining Applications," *IEEE Transactions on Geoscience and Remote Sensing*, **49**, 1, January 2011, pp. 451–461.
6. S. Meschino, L. Pajewski, M. Pastorino, A. Randazzo, and G. Schettini, "Detection of Subsurface Metallic Utilities by Means of a SAP Technique: Comparing

MUSIC- and SVM-Based Approaches," *Journal of Applied Geophysics*, **97**, October 2013, pp. 60–68.

7. A. De Coster, A. P. Tran, and S. Lambot, "Fundamental Analyses on Layered Media Reconstruction Using GPR and Full-Wave Inversion in Near-Field Conditions," *IEEE Transactions on Geoscience and Remote Sensing*, **54**, 9, September 2016, pp. 5143–5158.
8. A. R. Mangel, S. M. J. Moysey, and J. van der Kruk, "Resolving Precipitation Induced Water Content Profiles by Inversion of Dispersive GPR Data: A Numerical Study," *Journal of Hydrology*, **525**, June 2015, pp. 496–505.
9. M. Bevacqua, L. Crocco, L. D. Donato, T. Isernia, and R. Palmeri, "Exploiting Sparsity and Field Conditioning in Subsurface Microwave Imaging of Nonweak Buried Targets," *Radio Science*, **51**, 4, April 2016, pp. 301–310.
10. L. Di Donato and L. Crocco, "Model-Based Quantitative Cross-Borehole GPR Imaging via Virtual Experiments," *IEEE Transactions on Geoscience and Remote Sensing*, **53**, 8, August 2015, pp. 4178–4185.
11. C. Estatico, A. Fedeli, M. Pastorino, and A. Randazzo, "Microwave Imaging of Elliptically Shaped Dielectric Cylinders by Means of an L^p Banach-Space Inversion Algorithm," *Measurement Science and Technology*, **24**, 7, July 2013, p. 074017.
12. C. Estatico, A. Fedeli, M. Pastorino, and A. Randazzo, "Buried Object Detection by Means of a L^p Banach-Space Inversion Procedure," *Radio Science*, **50**, 1, January 2015, pp. 41–51.
13. C. Estatico, A. Fedeli, M. Pastorino, and A. Randazzo, "Quantitative Microwave Imaging Method in Lebesgue Spaces with Nonconstant Exponents," *IEEE Transactions on Antennas and Propagation*, **66**, 12, December 2018, pp. 7282–7294.
14. M. Pastorino and A. Randazzo, *Microwave Imaging Methods and Applications*, Boston, Artech House, 2018.
15. W. C. Chew, *Waves and Fields in Inhomogeneous Media*, Piscataway, NY, IEEE Press, 1995.